Received 18 May 2018; revised 15 July 2018; accepted 24 July 2018. Date of publication 15 August 2018; date of current version 31 August 2018.
The review of this paper was arranged by Editor M. Chan.

Digital Object Identifier 10.1109/JEDS.2018.2864791

Titanium Dioxide-Based Memristive Thin Film: A Correlation Study Between the Experimental Work and Simulation Program With Integrated Circuit Emphasis Hyperbolic Sine Models

RAUDAH ABU BAKAR[1], NUR SYAHIRAH KAMAROZAMAN[1], WAN FAZLIDA HANIM ABDULLAH[2], AND SUKREEN HANA HERMAN[1,2]

[1]NANO-Electronic Centre, Faculty of Electrical Engineering, Universiti Teknologi MARA, Shah Alam 40450, Malaysia
[2]Integrated Sensors Research Group, Faculty of Electrical Engineering, Universiti Teknologi MARA, Shah Alam 40450, Malaysia

CORRESPONDING AUTHOR: S. H. HERMAN (e-mail: hana1617@salam.uitm.edu.my)

This work was supported by the Ministry of Education Malaysia through Niche Research Grant Scheme under Project 600-RMI/NRGS 5/3 (7/2013).

ABSTRACT This paper presents a correlation study between experimental results of titanium dioxide (TiO_2)-based memristors and various hyperbolic sine function models. The current–voltage (I-V) characteristics of sol-gel-derived TiO_2 thin film annealed at 250°C were correlated with the reported hyperbolic sine function simulation program with integrated circuit emphasis memristor models. The correlation study showed that the existing models were not fitted well with our experimental data. The models with the lowest root means square errors were then combined together to achieve better fitting result. Further, experimental results of TiO_2 thin films fabricated by varying the annealing temperature at 350 °C and 450 °C were correlated to the proposed model to further elucidate the device operation. The parameters were then analyzed by multiplying and dividing the simulation results by two. It was found that both the Schottky and tunneling mechanisms had a significant impact in shaping the I-V characteristic of annealed TiO_2 thin film and device conductivity. The state variable derivative on the other hand caused changes in device threshold voltage. The knowledge gained from the fitting parameters of the proposed model enables us to predict the performance of fabricated memristive device and engineer the process parameters for desired memristive behavior.

INDEX TERMS Hyperbolic-based model, I-V characteristics, memristive device, titanium dioxide thin film.

I. INTRODUCTION

Memory resistor (memristor) is a fundamental passive element that was theoretically introduced to hold the relationship between flux and charge. As implied by its name, memristor can possibly remember its current resistance state without the applied voltage. The resistance value is highly dependent on the direction of current flowing through the device. Thus the memristor offers many advantages including non-volatility, low power consumption, a small size, fast speed, high volume density, and compatibility with conventional complementary metal-oxide semiconductor technology [1], [2]. Owing to its unique properties, the memristor can be incorporated in various applications including non-volatile memory, neuromorphic systems, programmable logic, and analog and microwave circuits [3]–[8]. Because of that, a lot of studies in memristor fabrication and simulation have been carried out to ensure successful integration in those applications [9]–[21].

Studies on memristor modeling have been performed to predict the memristor electrical properties for enabling successful implementation in various applications. The developed model should be able to incorporate nonlinearities and hysteretic behaviors of the memristor while also be tunable to fit with different types of memristor technologies [22]–[24]. Moreover, the model must have a closed form and high simulation speed and be precise, computationally efficient, and sufficiently accurate [23], [24].

Among the reported Simulation Program with Integrated Circuit Emphasis (SPICE) models that have been developed are the linear model, non-linear ionic drift model, tunneling-barrier model, and hyperbolic-sine-function-based memristor model [24]–[33]. Although several models are available to simulate the memristor electrical characteristic, only a few were developed based on the experimental data [29], [31], [34]. In [29], the SPICE model of a TiO_2 memristive device was modeled considering the effect of the tunnel barrier width in the metal–insulator–metal (MIM) structure. Unlike Abdalla and Pickett [29] and Chang *et al.* [31] offered a hyperbolic sine function model for tungsten oxide (WO_3)-based technology while Pino *et al.* [34] created a compact and simpler model for a memristor based on ion conductor chalcogenide. Amirsoleimani *et al.* [35] on the other hand, proposed a new physic based SPICE model that incorporates the charge transport mechanism in combination with tunneling and ohmic current conductions for Ag/TiO_2/ITO memristor. Regardless of their capability to mimic the characteristics of memristors, the extent to which the above models fit with other memristor technologies is not yet understood. Furthermore, the influence of the model parameters to the memristor characteristics and their relationship to fabrication condition is not discussed in detail.

This study was therefore performed to correlate the existing hyperbolic sine function memristor SPICE models with our experimental data. In this study, the models were initially correlated to sol-gel-derived spin-coated TiO_2 thin film annealed at various temperatures. The characterization data were obtained from [36]. The fitting process and the parameters analysis were conducted using Linear Technology Simulation Program with Integrated Circuit Emphasis (LTspice), a high performance SPICE simulator. The models with the least root means square (RMS) errors were chosen and combined for improvement. The influence of the proposed model parameters to the memristive characteristics and their relationship to fabrication conditions were then studied.

II. METHODOLOGY

A. DEVICE FABRICATION

The memristive device structure consisted of TiO_2 thin film sandwiched between platinum (Pt) electrode and indium-doped tin oxide (ITO) coated glass substrate (Pt/TiO_2/ITO glass), as shown in Fig. 1a. Two different mixtures were prepared using titanium (IV) isopropoxide (Ti[OCH(CH_3)$_2$]$_4$), glacial acetic acid (CH_3COOH), Triton X-100 ($C_{34}H_{62}O_{11}$), absolute ethanol (C_2H_5OH) and deionized water, which acted as the precursor, stabilizer, surfactant, and solvent, respectively to form the TiO_2 solution. Both mixtures were mixed together and stirred for 2 h to enable a complete chemical reaction. The TiO_2 solution was then spin-coated onto ITO glass substrate followed by deposition of Pt as a top electrode to form the memristive device. Prior to metal-contact deposition, the TiO_2 thin films were subjected to an annealing process for 20 min to enhance the films crystallinity. The varied parameter was the annealing temperature for each thin film, in which the annealing temperature was varied from 250°C to 450°C. The detailed fabrication method and results are reported in [36].

B. DEVICE CHARACTERIZATION

The current–voltage (I-V) characterization was performed by a two-point probe measurement method using a Keithley 4200 semiconductor characteristic system. The bias voltage was swept from 0 V to 5 V, followed by 5 V to −5 V, and returned to 0 V while simultaneously measuring the current. The applied voltages were applied to the top electrodes (Pt), while bottom electrode (ITO substrate) acted as the ground plane.

Fig. 1b shows the I-V characteristic of our spin-coated sol-gel-derived TiO_2 memristive thin film annealed at 250 °C for 20 min. The film thickness measured by surface profiler is 34.6 nm. As evident in the figure, the thin film exhibits resistive switching with an asymmetrical I-V characteristic. The curve obtained is pinched and crossed at the origin, which is the signature of a memristive device. From the I-V characteristic, the R_{ON} (ON state (low) resistance) and R_{OFF} (OFF state (high) resistance) were calculated as 51 and 137 Ω respectively at 4.11 V read voltage.

The dependency of memristive behavior on annealing temperature was also studied by performing the I-V characterization process on both TiO_2 thin films annealed at 350°C and 450°C respectively. The I-V characteristics for the annealed thin films are shown in Fig. 1c. As shown in the figure, the increase in the annealing temperatures results in the shrinkage of the switching loop area. It is believed that the degradation of the switching behavior was due to the improvement in film crystallization, as suggested by [3]. The crystallized film will form a larger grain size and cause oxygen vacancies to segregate to grain boundaries [31], [37]. Because oxygen vacancies transfer faster within the grain boundaries, the I-V characteristic with ohmic like behavior will be achieved as the temperature increases [31], [37]. Furthermore, annealed at a very high temperature will lower the Schottky barrier height, thereby enabling the electron transfer between the metal and oxide layers [38]. This will lead to the reduction in the switching loop area.

The surface morphology of annealed TiO_2 memristive thin film is shown in Fig. 2 (a-c). The field emission scanning electron microscopy images indicate that the samples exhibit a porous structure with non-uniform distribution of TiO_2 particles when annealing temperature increases from 250°C to 350°C. Annealed the film at 450°C however, resulted in a dense film morphology. The experimental results such as the resistance ratio and film thickness are subsequently used in the SPICE models.

C. DEVICE SIMULATION

In order to determine the best fitted SPICE model, the simulated I-V characteristic from the hyperbolic-sine function

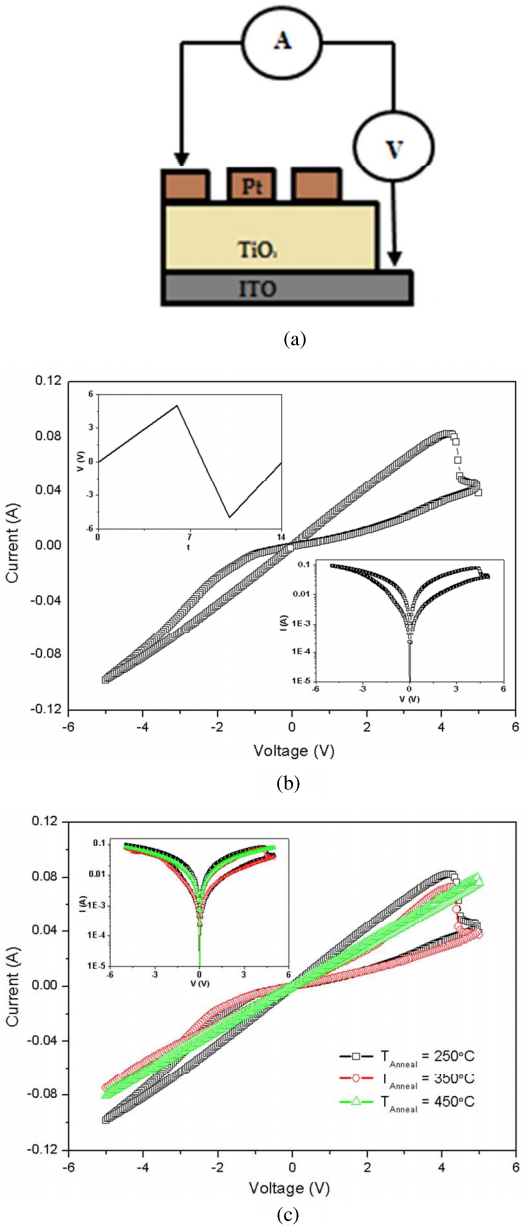

FIGURE 1. **(a) Device configuration of Pt/TiO_2/ITO glass substrate MIM structure and the measurement setup for IV characterization. (b) I-V characteristic of sol-gel-derived spin-coated TiO_2 thin film annealed at 250°C for 20 min [32]. The pinched hysteresis loop indicates the memristive device behavior. (Insets: Applied DC input voltage (upper). I-V characteristics in logarithmic scale (bottom)). (c) Experimental data for TiO_2 thin films annealed at 250, 350 and 450°C for 20 min in linear and logarithmic (inset) scales.**

based model were matched to the data obtained from [36]. The simulation process was performed using the 5 V sinusoidal input voltages. The matching parameters for each model were determined and the Root Means Square (RMS) errors were calculated by using,

$$e_{v,i} = \sqrt{\frac{1}{N}\left(\frac{\sum_{n=1}^{N}\left(v_{s,n}-v_{r,n}\right)^2}{\bar{v}_r^{-2}} + \frac{\sum_{n=1}^{N}\left(i_{s,n}-i_{r,n}\right)^2}{\bar{i}_r^{-2}}\right)} \quad (1)$$

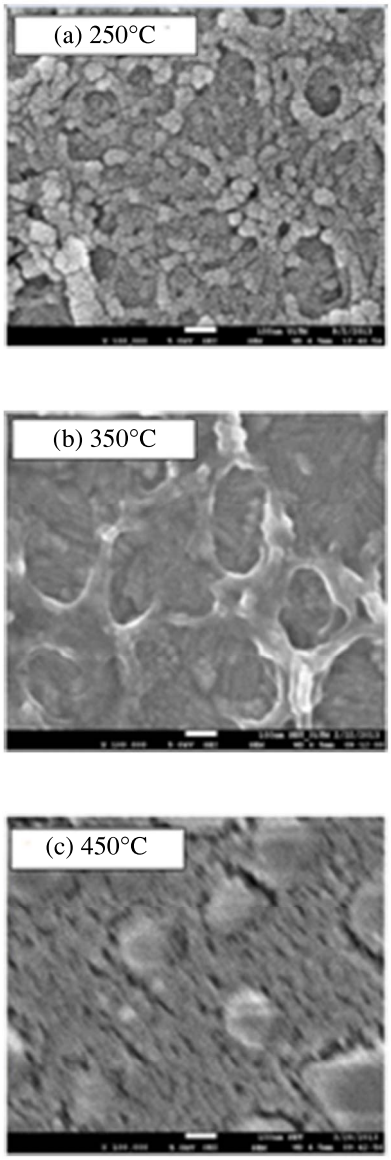

FIGURE 2. **Surface morphology of the deposited and annealed TiO_2 thin film at (a) 250°C, (b) 350°C and (c) 450°C for 20 min.**

where $\bar{v}_r$ and $\bar{i}_r$ are mean values of experimental data for voltage and current, v_s and i_s are the extracted voltage and current from the model simulation data, respectively [35]. The models with the lowest RMS error were then simulated with direct current (DC) sweep input to study the memristive performance using other input voltage. They are then combined together to further improved the SPICE model. The modified model was also correlated to other annealed thin films I-V characteristic to study the influence of proposed model parameters to the memristor characteristics and their relationship to fabrication conditions.

III. OVERVIEW OF HYPERBOLIC-SINE FUNCTION SPICE MEMRISTOR MODELS

Several SPICE models have been developed by employing the hyperbolic sinusoidal function to approximate the

electron tunneling through a thin MIM configuration and describe the non-linear dynamic of the memristor device. This model was obtained by considering the Schottky barrier at the interface of top electrode contact and TiO_2 and the ohmic contact at the interface of bottom electrode and TiO_{2-x} [39]. Applying a positive voltage resulted in the drifting of oxygen vacancies towards bottom electrode and subsequently narrowed the Schottky barrier and thus causing the tunneling current to dominate. This will therefore turn the device ON. Whereas, a negative voltage application repelled away the oxygen vacancies from the top electrode, hence, increases the Schottky barrier height and switched the device OFF.

Some of these models are Laiho *et al.* [30], Chang *et al.* [31], Eshragian *et al.* [32], and Yakopcic *et al.* [33] models. Laiho *et al.* [30] represents both I-V relationship and state variable function using the hyperbolic sinusoidal function, which are given by the following equations

$$I(t) = \begin{cases} a_1 w(t) \sinh(b_1 V(t)), & V(t) \geq 0 \\ a_2 w(t) \sinh(b_2 V(t)), & V(t) < 0 \end{cases} \quad (2)$$

$$\frac{dw}{dt} = \begin{cases} c_1 w(t) \sinh(d_1 V(t)), & V(t) \geq 0 \\ c_2 w(t) \sinh(d_2 V(t)), & V(t) < 0 \end{cases} \quad (3)$$

where a_1, a_2, b_1 and b_2 are used to adjust the I-V response, while c_1, c_2, d_1 and d_2 are used to shape the threshold and intensity of the state. Biolek's window function ($F(w(t))$ was later added by [42] to the state variable function to set the device boundary ($0 \leq w(t) \leq 1$).

$$\frac{dw}{dt} = \begin{cases} c_1 w(t) \sinh(d_1 V(t)) F(w(t)), & V(t) \geq 0 \\ c_2 w(t) \sinh(d_2 V(t)) F(w(t)), & V(t) < 0 \end{cases} \quad (4)$$

As the rate of change of the state variable is highly dependent on the drift of oxygen vacancies within the active region of the memristor, thus the sinh-shaped function was used to assume the non-linearity dependency on the applied voltage. This consequently leads to the yield of a programming device threshold [32]. Although Laiho's model offers simplicity, it cannot predict the device physic perfectly [40].

An alternative model that likewise generalizes the hyperbolic sinusoidal function was developed by Chang *et al* [31]. The I-V relationship and state variable function are described by the following equations:

$$I(t) = (1 - w(t))\, \alpha \left\lfloor 1 - e^{\beta V(t)} \right\rfloor + w(t)\, \gamma \sinh(\delta V(t)) \quad (5)$$

$$\frac{dw}{dt} = \lambda \left[\eta_1 \sinh(\eta_2 V(t)) \right] \quad (6)$$

It is apparent that, the I-V relationship is the combination of the Schottky barrier effect between the tungsten oxide layer and bottom electrode and the tunneling effect through the MIM junction. Based on equation (5) the Schottky conduction becomes dominant if the state variable, $w(t)$ is zero and vice versa when $w(t)$ is 1. The state variable function, on the other hand, is similar to (3), in which η_1, η_2 and λ are the fitting parameters used to shape the dynamics of the state variable equation [41]. The state variable function is then modified by adding an ion diffusion term to (6) to account for the natural oxygen vacancy (V_{ox}) diffusion [41]. The new equation is defined as:

$$\frac{dw}{dt} = \lambda \left[\eta_1 \sinh(\eta_2 V(t)) - \frac{w(t)}{\tau} \right] \quad (7)$$

where τ is a time constant on the order of a few seconds.

As Chang *et al.* also used sinh-shaped function to model the non-linearity behavior within memristor. Compared with the existing models, the state variable, w was now described by the cross section area of the conductive region developed due to the drift of oxygen vacancies. Thus, the formation of new conductive region does not affected by the existing conductive region. Because of this, the rate of change of the state variable is highly dependent only on the applied voltage [31].

Compared to previous SPICE models, Eshragian's model [32] provides a detailed study on the memristor conduction mechanism. Furthermore, it addresses the programming threshold issue, memristive operation regime limits and convergence and overflow problems. In this model, the state variable derivative is linearly related to the tunneling phenomenon. It is developed by describing the nonlinear dynamics of the memristor device using the following form:

$$\frac{dw}{dt} = v \cdot g(V, \rho(w), \varphi_0) \quad (8)$$

where v is a constant value to identify the ON and OFF switching speed in a normalized distance ($w \in (0,1)$) based on experimental result, and the $g(V, \rho(w) \varphi_0)$ function is used in the symmetric or asymmetric curve for both negative and positive voltages. In addition, $\rho(w)$ is a shape factor function and φ_0 is the equilibrium ($V \equiv 0$) barrier height in eV. The $g(V, \rho(w), \varphi_0)$ and $\rho(w)$ functions are given by,

$$g(V, \rho(w), \varphi_0) = \left(1 - \frac{V}{2\varphi_0}\right) e^{\left(\rho(w)\varphi_0\left(1-\sqrt{1-\frac{V}{2\varphi_0}}\right)\right)} - \left(1 + \frac{V}{2\varphi_0}\right) e^{\left(\rho(w)\varphi_0\left(1-\sqrt{1+\frac{V}{2\varphi_0}}\right)\right)} \quad (9)$$

$$\rho(w) = \delta + \eta\left(1 - (2w-1)^{2p}\right) \quad (10)$$

where δ is an offset (positive) constant, η is a positive coefficient to control the $\rho(w)$ nonlinearity and $1 - (2w-1)^{2p}$ is a normalized nonlinear function that describes the nonlinear conditions at the boundaries. By tuning the shape factor resulted in the programmed of several thresholds [32]

The current–voltage relationship on the other hand employs the model introduced by Yang *et al.* [42] and is represented by

$$i_M = a_1 \sinh(b_1 V_M) + a_2\left(e^{(b_2 V_M)} - 1\right) \quad (11)$$

where a_1 and b_1 are fitting parameters for characterizing the ON state and are based on electron tunneling through a barrier. Additionally, a_2 and b_2 are used as fitting parameters to characterize the net electronic barrier for the OFF

state. These fitting parameters are constant values, dimensionless and depended on physical properties of the material of memristor [42], [43]. As suggested by [43], the model equation in (11) can be compared to the following theoretical expression,

$$I = 2nqve^{\left(-\frac{\phi_B}{k_0T}\right)} \sinh\left(\frac{aq}{k_0Td}V\right) + SA^*T^2e^{\left(-\frac{\phi_B}{k_0T}\right)}\left(e^{\left(\frac{qV}{k_0T}\right)} - 1\right) \quad (12)$$

where, n is electrons, q is electronic charge (1.6×10^{-19} C), v is the probability of electron transition without the barrier, Φ_B is barrier height, k_0 is Boltzmann constant, T is temperature, d is thickness of oxide layer, S is the area of the electrode and A^* is the effective Richardson constant.

As Eshragian *et al*'s model [32], Yakopcic *et al*'s model [33] also described his device model by three main characteristics which are electron tunneling, non-linear ion drift and voltage threshold. Yakopcic *et al*'s I-V relationship is expressed by the approximation of electron tunneling using the hyperbolic sine function, as previously proposed in [30]. The state variable changes, on the other hand depend on the product of two functions, $g(V(t))$ and $f(w(t))$ as in (13). The function $g(V(t))$ is responsible for the effect of threshold voltage in the memristive device, while $f(w(t))$ is used to model the nonlinear ion drift. Accordingly, these are given by the following expressions:

$$\frac{dw}{dt} = \eta\left(gV\left(t\right)\right)\left(fw\left(t\right)\right) \quad (13)$$

$$g\left(V\left(t\right)\right) = \begin{cases} A_p\left(e^{V(t)} - e^{V_p}\right), & V\left(t\right) > V_p \\ -A_n\left(e^{-V(t)} - e^{V_n}\right), & V\left(t\right) < -V_n \\ 0, & -V_n \le V\left(t\right) \le V_p \end{cases} \quad (14)$$

$$f\left(w\right) = \begin{cases} e^{-\alpha_p\left(w-w_p\right)}m_p\left(w, w_p\right), & w \ge w_p \\ 1, & w < w_p \end{cases} \quad (15)$$

$$f\left(w\right) = \begin{cases} e^{\alpha_n\left(w+w_n-1\right)}m_n\left(w, w_n\right), & w \ge 1 - w_n \\ 1, & w < 1 - w_n \end{cases} \quad (16)$$

where A_p and A_n are the parameters that are used to control the ion motion speed, and V_p and V_n represent the threshold voltages. In addition, α_p, α_n, x_p and x_n are the parameters that determine where the state variable motion is no longer linear and the degree to which the state variable motion is dampened. Moreover, $m_p(w, w_p)$ and $m_n(w, w_n)$ are the window function, which can be described by

$$m_p\left(w, w_p\right) = \frac{w_p - w}{1 - w_p} + 1 \quad (17)$$

$$m_n\left(w, w_n\right) = \frac{w}{1 - w_n}. \quad (18)$$

IV. SIMULATION OF HYPERBOLIC-BASED MEMRISTOR MODEL

A. SIMULATION OF LAIHO, CHANG, ESHRAGIAN AND YAKOPCIC SPICE MODELS

As previously defined, both Laiho *et al.* [30] and Yakopcic *et al.* [33] suggested that the device conductivity depends on the change of resistance provided by the state variable $w(t)$. As shown in Fig. 3a, using the Laiho SPICE model results in the highest RMS error. This is due to the

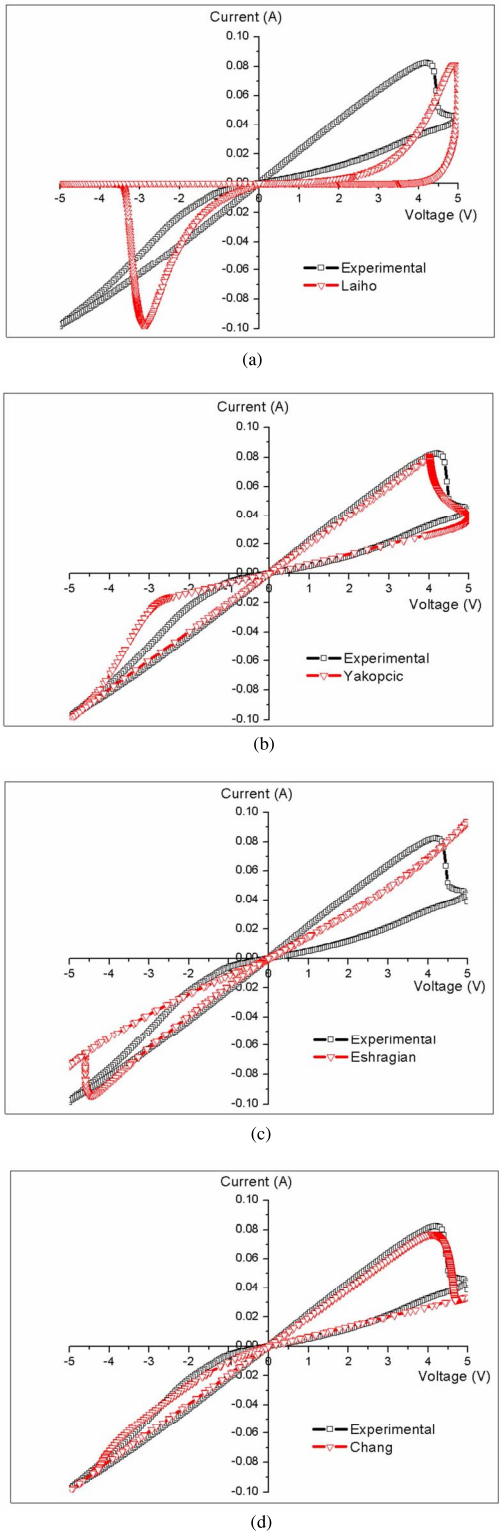

FIGURE 3. Simulation results when modeling the sol-gel derived spin coated TiO_2 thin film annealed at 250°C for 20 min: using (a) Laiho (b) Yakopcic (c) Eshragian (d) Chang SPICE models for a sinusoidal input of 5 V.

TABLE 1. The Relative Root Mean Square Errors of Various SPICE Models With the Experimental Data.

Model	Model Parameters	RMS Errors	Ref.
Non-linear Ion Drift	f =1 Hz, R_{ON} = 51 Ω, R_{OFF} = 137 Ω, D = 34.6 nm, R_{init} = 50 Ω and $\mu_v = 1\times10^{-14}$ $m^2s^{-1}V^{-1}$	2.95	[25]
	f =1 Hz, R_{ON} = 51 Ω, R_{OFF} = 137 Ω, D = 34.6 nm, R_{init} = 50 Ω, p = 1 and $\mu_v = 1\times10^{-14}$ $m^2s^{-1}V^{-1}$	2.66	[26]
	f =1 Hz, R_{ON} = 51 Ω, R_{OFF} = 137 Ω, D = 34.6 nm, R_{init} = 50 Ω, p = 7 and $\mu_v = 3\times10^{-14}$ $m^2s^{-1}V^{-1}$	2.46	[27]
	f =1 Hz, R_{ON} = 51 Ω, R_{OFF} = 137 Ω, D = 34.6 nm, R_{init} = 50 Ω, p = 1 and $\mu_v = 3.5\times10^{-14}$ $m^2s^{-1}V^{-1}$	0.82	[28]
ThrEshold Adaptive Memristor Model (TEAM)	$k_{off} = 0.05$, $k_{on} = 2$, $i_{off} = 30\times10^{-3}$, $i_{on} = 80\times10^{-3}$, $\alpha_{off} = 3$, $\alpha_{on} = 3$, $a_{off} = 0.275$, $a_{on} = 70$, $x_{off} = 52$, $x_{on} = 5.6$, $w_c = 0.95$, $x_{init} = 1.21$, and $\lambda = 0.988$	1.42	[24]
Hyperbolic-Sine Function Based Model	$a_1 = 7.5\times10^{-4}$, $b_1 = 1.2$, $a_2 = 1.05\times10^{-2}$, $b_2 = 1.2$, $c_1 = 6\times10^{-4}$, $d_1 = 2$, $c_2 = 6.6\times10^{-4}$, $d_2 = 3.8$, $x_0 = 0.001$, $p = 2$	4.84	[30]
	$\alpha = 3.195$, $\beta = 6.505\times10^{-3}$, $\gamma = 2.45\times10^{-1}$, $\delta = 3.25\times10^{-2}$, $x_{max} = 0.95$, $x_{min} = 0.05$, $drift\_bit = 150$, $\lambda = 0.06$, $\eta_1 = 12.5\times10^{-6}$, $\eta_2 = 4$, $\tau = 1$	0.13	[31]
	$a_1 = 5.7\times10^{-2}$, $a_2 = 0.5$, $b_1 = 0.25$, $b_2 = 5\times10^{-4}$, $p = 1$, $f_{off} = 2$, $f_{on} = 0.02$, $sfo = 0.2$, $sfm = 0.05$, $w_{min} = 0.01$, $w_{max} = 0.95$, $p_0 = 1.3$, $n = 0.05$, $w_{init} = 0.05$	1.34	[32]
	$a_1 = 0.40$, $a_2 = 0.395$, $b = 0.05$, $V_p = 4$, $V_n = 2.5$, $A_p = 55.5$, $A_n = 1.95$, $x_p = 0.3$, $x_n = 0.025$, $\alpha_p = 1.55$, $\alpha_n = 12.5$, $x_o = 0.99$, and $\eta = -1$	0.50	[33]

use of basic generic equation of sinh function in equation (2) and (3) which is incapable to reflect the actual devices behavior [44]. Improving the state variable function by incorporating the threshold voltage effects (13) leads to a better fitted I-V characteristic as achieved by Yakopcic *et al.* (Fig. 3b).

Chang *et al.* [31] and Eshragian *et al.* [32] on the other hand proposed that the I-V relationship in memristive devices is basically due to the combination of Schottky and tunneling effects at the MIM junction. Although Eshragian's model offers improvement in current overflow and convergence problems, it is unable to correlate well with the experimental data. Using $a_1 = 5.7\times10^{-2}$, $a_2 = 0.5$, $b_1 = 0.25$, $b_2 = 5\times10^{-4}$, $p = 1$, $f_{off} = 2$, $f_{on} = 0.02$, $sfo = 0.2$, $sfm = 0.05$, $w_{min} = 0.01$, $w_{max} = 0.95$, $p_0 = 1.3$, $n = 0.05$, and $w_{init} = 0.05$ results in an asymmetrical I-V characteristic (Fig. 3c). Compared to the other hyperbolic function models discussed herein, Chang *et al.* gives an I-V curve that is best fitted to the experimental data (Fig. 3d). This presumably on account of the inclusion of the ion diffusion term, $\frac{w(t)}{\tau}$, in its their state variable derivative function. The root means square error is calculated as 0.13.

All of the above showed our attempts to correlate an asymmetrical I-V characteristic of a memristor based on TiO_2 thin film with hyperbolic-based SPICE models. Table 1 summarizes the fitting parameters and relative RMS errors of the models with the experimental data. As summarized in Table 1, both Chang and Yakopcic models resulted in the smallest RMS errors. Because of that, both models were further simulated at different frequencies and using a DC input voltage for models validation.

Fig. 4(a) and (b) display the sinusoidal V(t) and I(t) plots (upper inset), memristances (bottom inset) and I-V characteristics simulated using both Chang and Yakopcic models at various frequencies. As apparent in the inset graphs the non-linear conducting behavior is clearly seen in both models' I(t) characteristics. The memristances were calculated as 115 and 145 Ω respectively. It also observed that simulating Chang and Yakopcic models at 1 and 100 Hz resulted in the decrease of hysteresis loop area leading to the behavior of linear resistor. Since one of memristor's attributes is the shrink of the hysteresis loop area at higher frequencies [44], thus both Chang and Yakopcic SPICE models can be used to model memristor.

Fig. 5 shows the simulation results when simulating the Chang and Yakopcic models to DC input voltage. As apparent in Fig. 5a and b, both models cannot properly match the device experimental data. The hysteresis loop for Chang model seems to disappear with the applied of negative voltages while a bigger loop was obtained using Yakopcic model.

B. SIMULATION OF CHANG AND YAKOPCIC COMBINATION MODEL

Since Chang and Yakopcic models show the best fitted I-V behavior as compared to experimental data, both models were combined together to further improve the performance of the SPICE model. In this combination, Chang's current–voltage relationship (equation (5)) is incorporated into Yakopcic's state variable model (equation (13)). As previously reported, in TiO_2 metal-insulator-metal configuration, the conduction mechanism that could be possibly occurred are the Schottky emission and tunneling

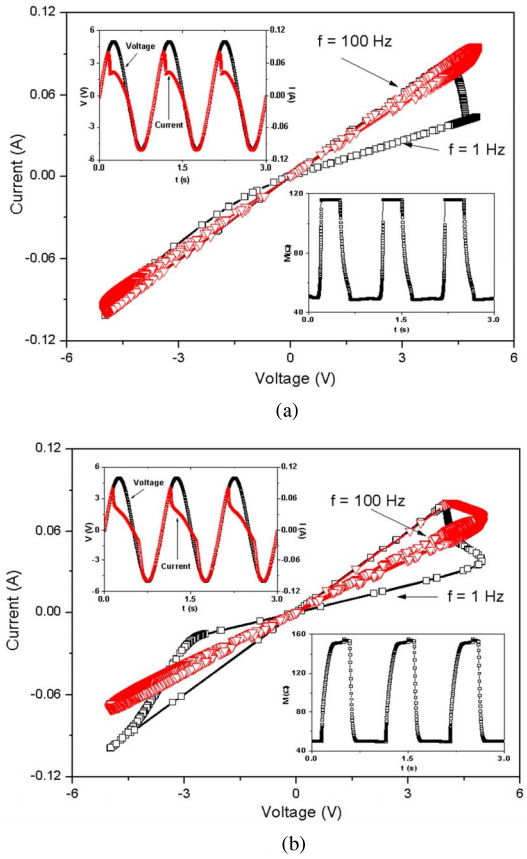

FIGURE 4. Simulation results when modeling the device using (a) Chang and (b) Yakopcic SPICE models at different frequencies. The upper and bottom insets in (a) and (b) show the current and voltage sinusoidal input at frequency = 1 Hz and the memristance values.

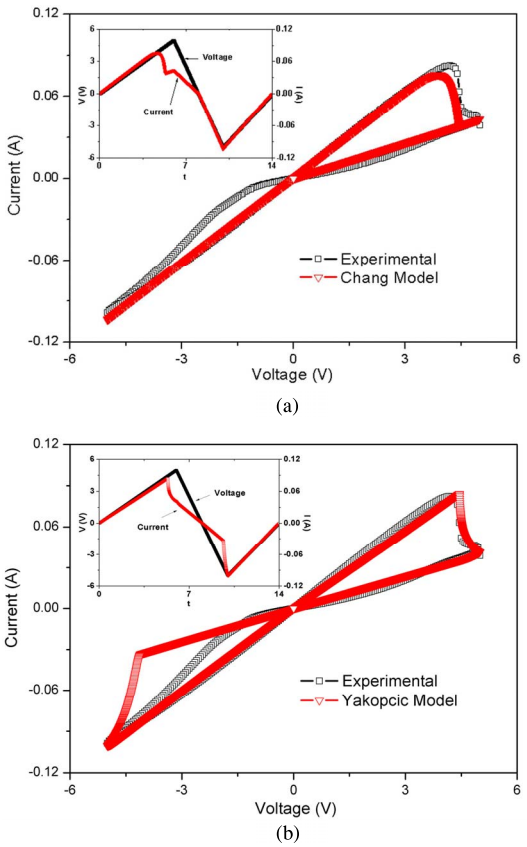

FIGURE 5. Simulation results when modeling the device with DC sweep input: The plots show the I-V characteristics simulated using (a) Chang and (b) Yakopcic SPICE models. The inset in (a) and (b) show the DC input current and voltage waveforms. In this simulation the fitting parameters for Chang and Yakopcic models are: $\alpha = 3.235$, $\beta = 6.525\times10^{-3}$, $\gamma = 2.45\times10^{-1}$, $\delta = 3.25\times10^{-2}$, $x_{max} = 0.95$, $x_{min} = 0.05$, $drift\_bit = 275$, $\lambda = 0.275$, $\eta_1 = 10.5\times10^{-6}$, $\eta_2 = 4$, $\tau = 1$ and $a_1 = 0.395$, $a_2 = 0.405$, $b = 0.05$, $V_p = 4.45$, $V_n = 4.1$, $A_p = 45.5$, $A_n = 5.55$, $x_p = 0.0124$, $x_n = 5\times10^{-6}$, $\alpha p = 3.55$, $\alpha_n = 14.85$, $x_o = 0.95$, and $\eta = -1$ respectively.

current [35], [43], [45]–[48]. In Section III, it has been mentioned that the occurrence of Schottky behavior is apparently due to the formation of Schottky barrier between TiO_2 and ITO layers. Under biased condition however, the conduction mechanism is dominated by tunneling current. This is because of the drift of oxygen vacancies will narrow the Schottky barrier height and subsequently increase the current [43]. Because of the similarity between our device structure and Chang's MIM configuration, the equation (5) was chosen to describe the current transport mechanism.

The Yakopcic's state variable model on the other hand was used in this proposed model due to the inclusion of built in threshold in the model that will enable the new improved model to include the effect of non-linear kinetics in resistive switches [40]. Eventhough the dynamic behavior of charge transport is not accurately presented in [33], no changes were made in our proposed model. This issue will be addressed in detail in our future study.

The model was simulated using both sinusoidal and DC sweep inputs. The simulation results were demonstrated in Fig. 6 and 7 respectively. It can be seen in Fig. 6a and 7a that the model exhibits a good agreement with the results from the experimental data. The RMS error was calculated to be 0.05. As apparent in the both figures, the proposed model could compensate the problems causing by the individual model and subsequently produce a well fitted memristive behavior. To further verify the validity and the quality of the SPICE model, the I-V characteristics were plotted in semi-log scale graph as shown in Fig. 6b and 7b. It is observed that the reset and set transitions start near 4.32 and −5 V respectively for both simulation and experimental values. Therefore, it is suggested that the reset and set processes are accurately captured by the proposed model.

The memristance values were calculated to be 133 Ω and 125 Ω when simulated with sinusoidal and DC sweep inputs respectively. The model also showed a shrinking of the hysteresis loop at higher frequencies as seen in Fig. 8. The I-V curve tends to diminish as the frequency increases to 100 Hz. Because of the proposed model achieved the smallest RMS errors, this model was chosen for comparison to other experimental data to relate the fitting parameters in the equations to the process parameter variations.

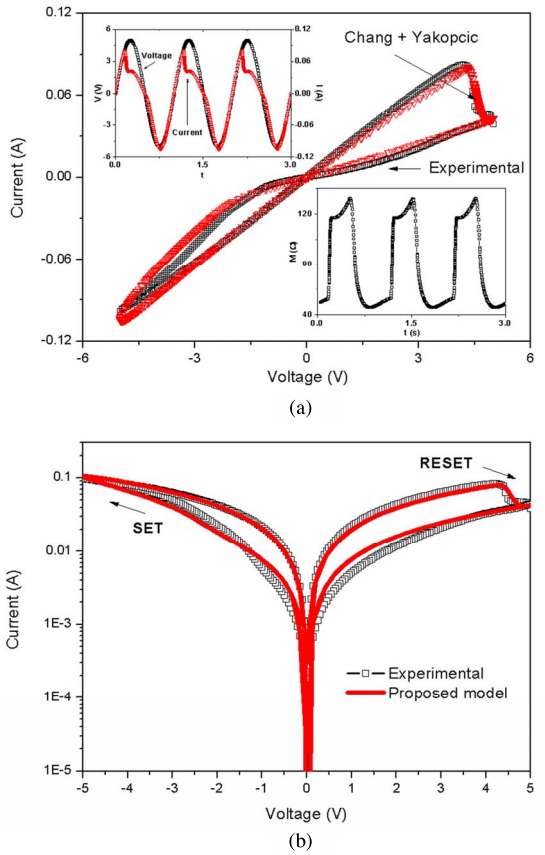

FIGURE 6. Proposed SPICE model simulation in comparison with fabricated Pt/TiO_2/ITO memristor plotted in (a) linear and (b) semi-log scales. The plot shows the simulation result of proposed model when simulating with the following parameters: $\alpha = 0.533$, $\beta = 0.0443$, $\gamma = 0.9051$, $\delta = 0.0132$, $V_p = 4.25$, $V_n = 0.1055$, $A_p = 1.296$, $A_n = 0.5155$, $x_p = 0.4753$, $x_n = 0.2255$, $\alpha_p = 0.2255$, $\alpha_n = 7.275$, $x_o = 0.195$, and $\eta = 2.05$ respectively. The upper and bottom inserts display the sinusoidal voltage input, the memristor current and the memristance values versus time respectively.

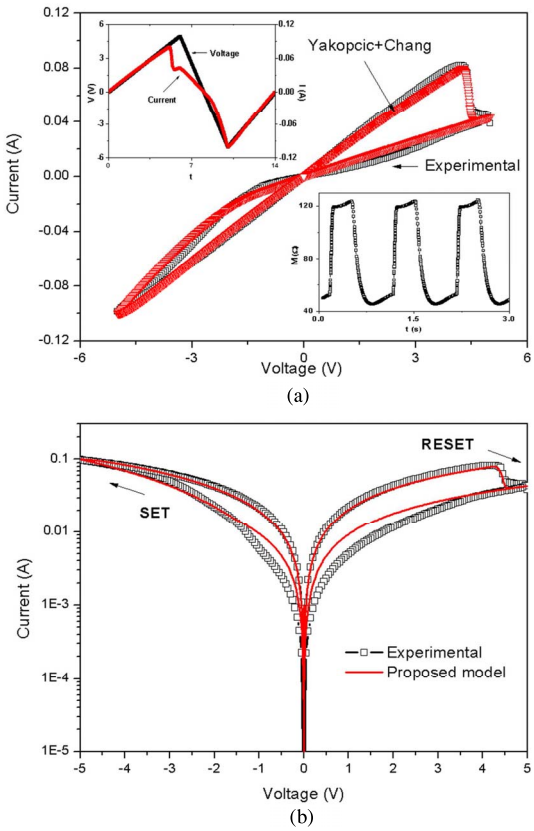

FIGURE 7. Simulation results when modeling the device using proposed model with DC sweep input plotted in (a) linear and (b) semi-log scales: The plots display the comparison between the model and experimental data. The upper and bottom insets are the DC input voltage and output current waveforms and memristance values versus time. In this simulation the I-V curve demonstrate a close match to the experimental data. The fitting parameters for the proposed model are: $\alpha = 0.4075$, $\beta = 0.0515$, $\gamma = 0.4475$, $\delta = 0.0128$, $V_p = 4.25$, $V_n = 2.075$, $A_p = 0.3775$, $A_n = 0.3928$, $x_p = 0.730$, $x_n = 0.019$, $\alpha_p = 1.55$, $\alpha_n = 4.9155$, $x_o = 0.0013$, and $\eta = 0.75$ respectively.

V. MODEL PARAMETERS ANALYSIS

The proposed simulation model was then compared to the I-V characteristic of three TiO_2 thin film samples annealed at 250°C, 350°C, and 450°C for 20 min, respectively, to further evaluate the relationship between the model parameters and fabrication process conditions. Fig. 9 shows the simulation results when modeling the annealed thin films using the proposed model while Table 2 summarizes the fitting parameters for the films. The simulation was carried out with DC sweep input. As summarized in the table, the parameters that describe the current–voltage relationship (α, β, γ and δ) and state variable (A_p, A_n, x_p, α_n and x_0) of memristive device play a significant role in the determination of a well-fitted behavior. It is evident that, the increases in annealing temperature lead to the reduction in the model parameters and subsequently lead to smaller hysteresis loop. Thus, the effect of the parameter models on the memristor characteristic is analyzed. The analysis was divided into the current–voltage relationship and state variable parameter effects. The parameters were varied by multiplying and dividing the fitting parameters for TiO_2 thin film annealed at 250°C by either two or four to evaluate

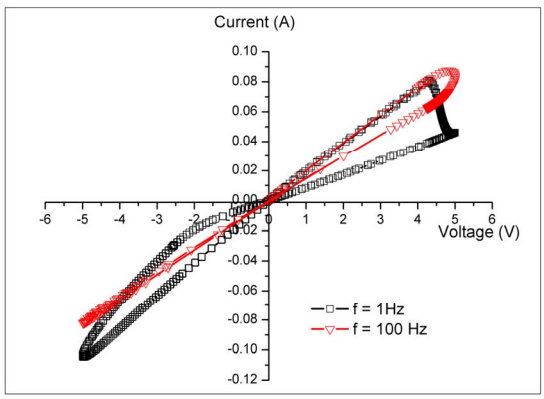

FIGURE 8. Memristive device behavior simulated using proposed SPICE model with 5 V sinusoidal input voltages at 1 and 100 Hz frequency.

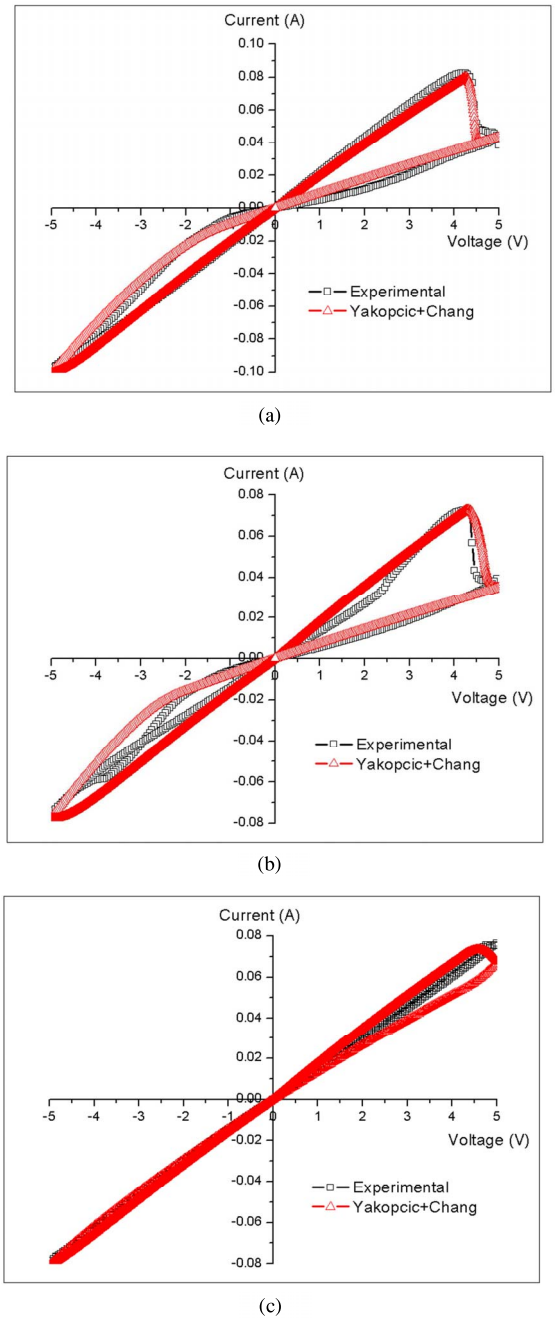

FIGURE 9. Simulation results when modeling the TiO_2 thin film using Chang's SPICE model for a sinusoidal input of 5 V and annealed at (a) 250°C, (b) 350°C, and (c) 450°C.

the change in the I-V curve shape. While the parameter under test was varied, the other parameters will remain the same [39], [49]. The R_{ON} and R_{OFF} under a voltage of 4.11 V are then computed.

A. THE CONDUCTION PARAMETER EFFECTS

The graphs shown in Figs. 10 a and b indicate that the variations in the values of α and β have a significant impact on the area of the hysteresis loop and the maximum positive and negative currents. From the I-V characteristics we can see that as the values of α and β increase, the hysteresis loop

TABLE 2. Fitting Parameters of Proposed SPICE Model for TiO_2 Thin Film Annealed at 250°C, 350°C and 450°C.

	250°C	350°C	450°C
α	0.4075	0.3808	0.3707
β	0.0515	0.0502	0.0502
γ	0.4475	0.3948	0.3969
δ	0.0128	0.0091	0.0129
V_p	4.250	4.250	4.250
V_n	2.075	2.075	2.075
A_p	0.3775	0.0775	0.0108
A_n	0.3928	0.0928	0.0523
x_p	0.730	0.673	0.373
x_n	0.019	0.019	0.010
α_p	1.550	1.550	1.550
α_n	4.916	5.0916	5.0155
x_0	0.0013	0.0129	0.0129

becomes larger. In contrast, shrinking of the loop is observed when α and β decrease to 0.2038 and 0.0258, respectively. The maximum positive and negative currents were measured to be 0.165 and −0.199 A respectively when α is multiplied by two. While the currents are 0.147 and −0.227 A with the increases of β. The changes in the current will then cause the changes in the memristor resistance. Table 3 summarized the R_{ON}, R_{OFF} and R_{OFF}/R_{ON} ratio for α and β values multiplied and divided by two. It is apparent from this table that high resistance ratio can be achieved using high value of α and β.

As described in Section III, the current–voltage relationship in Chang's SPICE model is accounted for both Schottky and tunneling conduction mechanisms. Assuming that the charge transport during the OFF state is due to thermionic emission current, the Schottky mechanism is thus given as follows [49]–[51]

$$I = SA^*T^2 \exp\left(-\frac{q\phi_B}{kT}\right) \exp\left(\frac{q}{nkT}\right)\left[1 - \exp\left(-\frac{qV}{kT}\right)\right] \tag{19}$$

Comparing the first term in equation (5) with equation (19), the parameters α and β can hence be regarded as $SA^*T^2 \exp(-\frac{q\phi_B}{kT}) \exp(\frac{q}{nkT})$ and $-\frac{q}{kT}$ respectively.

From the equation (19), both α and β are influenced by the change of temperature, T. If the doping concentration in TiO_2 layer is low and voltage is constant, the drift mobility is affected by the lattice scattering due to the thermal vibration of atoms. The increases in temperature will result in higher lattice scattering and subsequently decrease the drift mobility [43], [52]. As the drift mobility decreases, the resistivity increases resulting in small current. Since β is inversely related to temperature, thus the increases in temperature will reduce the value of β and causes the reduction in current. The value of α on the other hand increases with the increase of temperature because of its linear relationship to T^2.

However, if the temperature is a constant value, the parameter α is therefore determined by the electrode area, S, barrier

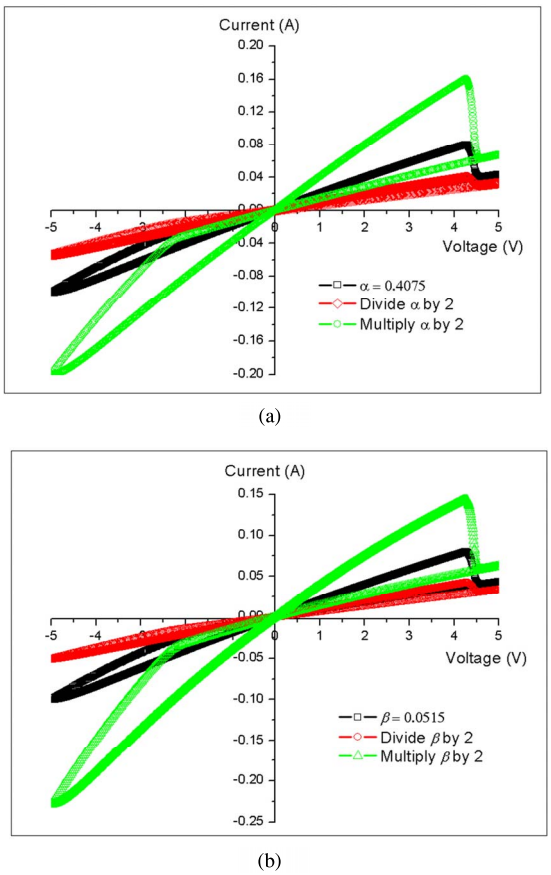

FIGURE 10. I-V characteristic of TiO_2 thin film annealed at 250°C for 20 min simulated using variations of α and β values: where (a) $\alpha = 0.2038$ and 0.815 (b) $\beta = 0.02575$ and 0.103. In this simulation $\gamma = 0.4475$, $\delta = 0.0128$, $V_p = 4.25$, $V_n = 2.075$, $A_p = 0.3775$, $A_n = 0.3928$, $x_p = 0.730$, $x_n = 0.019$, $\alpha_p = 1.55$, $\alpha_n = 4.916$ and $x_0 = 0.0013$.

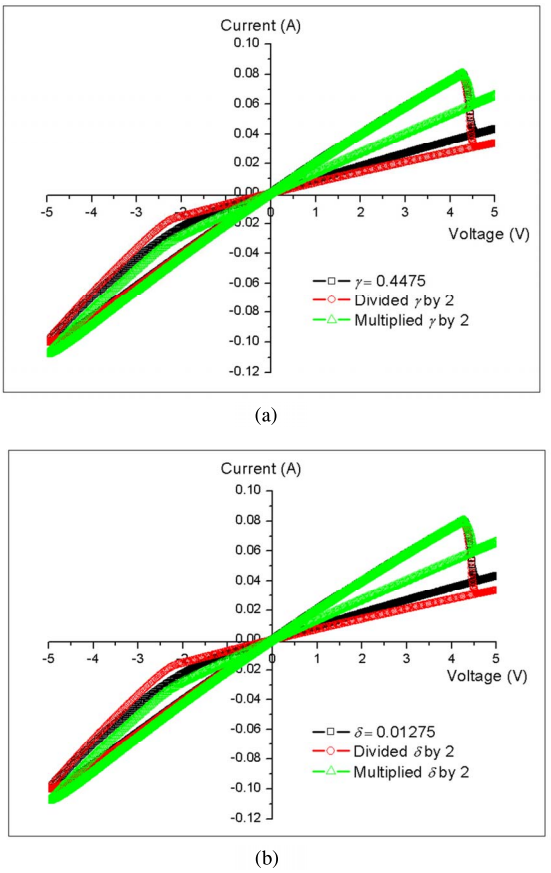

FIGURE 11. I-V characteristic of TiO_2 thin film annealed at 250°C for 20 min simulated using variations of γ and δ values: where (a) $\gamma = 0.22375$ and 0.895 (b) $\delta = 0.006375$ and 0.0255. In this simulation $\alpha = 0.4075$, $\beta = 0.0515$, $V_p = 4.25$, $V_n = 2.075$, $A_p = 0.3775$, $A_n = 0.3928$, $x_p = 0.730$, $x_n = 0.019$, $\alpha_p = 1.55$, $\alpha_n = 4.916$ and $x_0 = 0.0013$.

height, ϕ_B and ideality factor, n. The increases in the electrode area, S will result in the increases of α and subsequently the thermionic current. This is because of proportionally related between α and electrode area. Unlike electrode area, α is exponentially proportional to the barrier height, ϕ_B.

Theoretically, ϕ_B is a potential energy that will determine the rectifying behavior between metal and semiconductor junction. As a result, controlling the magnitude of this barrier is of vital importance in the determination of device electrical characteristics to ensure successful implementation of semiconductor device in various applications. Modification of ϕ_B can be achieved by finding the suitable metal or compound that produces the desired barrier height [53]–[56]. Since, barrier height is a structural dependence parameter, modifying the interface structure of the metal-semiconductor interface could possibly tune the magnitude of ϕ_B [56]. This can be achieved by inserting of organic molecular dipoles, insulating materials or monolayers of inorganic atoms, impurities or defects at the metal-semiconductor interface [57]. It is also reported that surface [58] and thermal [50], [59]–[61] treatments on the semiconductor led to the changes in the barrier height. The findings of the current studies are consistent with those of other studies which showed that by subjecting the semiconductor interface to annealing process will subsequently modify the barrier height [50], [59]–[61]. An increase of α could then be achieved by lowering the barrier height resulting in the increases of current. When comparing the two plots in Figs 10a and 10b, the decreases in the Schottky barrier height prove the suggestion made by [33], in which the lowering of barrier height causes the electron movement in the MIM structure and therefore contributes to the change of the I-V curve.

The ideality factor, n on the hand is used to examine the transport mechanism within the device [62]. The occurrence of pure thermionic emission can be detected if $n = 1$. However, other transport mechanisms may be present if n is larger than unity [50]. The ideality factor can be determined from the slope of the linear region of the forward bias ln (J)-V using

$$n = \frac{q}{kT}\left(\frac{dV}{d\,(\ln J)}\right) \tag{20}$$

where J is the current density. As α is an exponentially dependence on the reciprocal of n, higher value of n consequently lead to the decrease of α and current.

TABLE 3. R_{ON} and R_{OFF} With α and β Multiplied and Divided by Two.

		α and β divided by two		α and β multiplied by two	
	SIMULATION DATA FOR 250°C	α (0.2038)	β (0.0258)	α (0.815)	β (0.103)
R_{ON} (Ω)	52.97	105.79	100.71	26.38	29.17
R_{OFF} (Ω)	113.29	149.45	146.47	72.86	77.58
R_{OFF}/R_{ON}	2.14	1.41	1.45	2.76	2.66

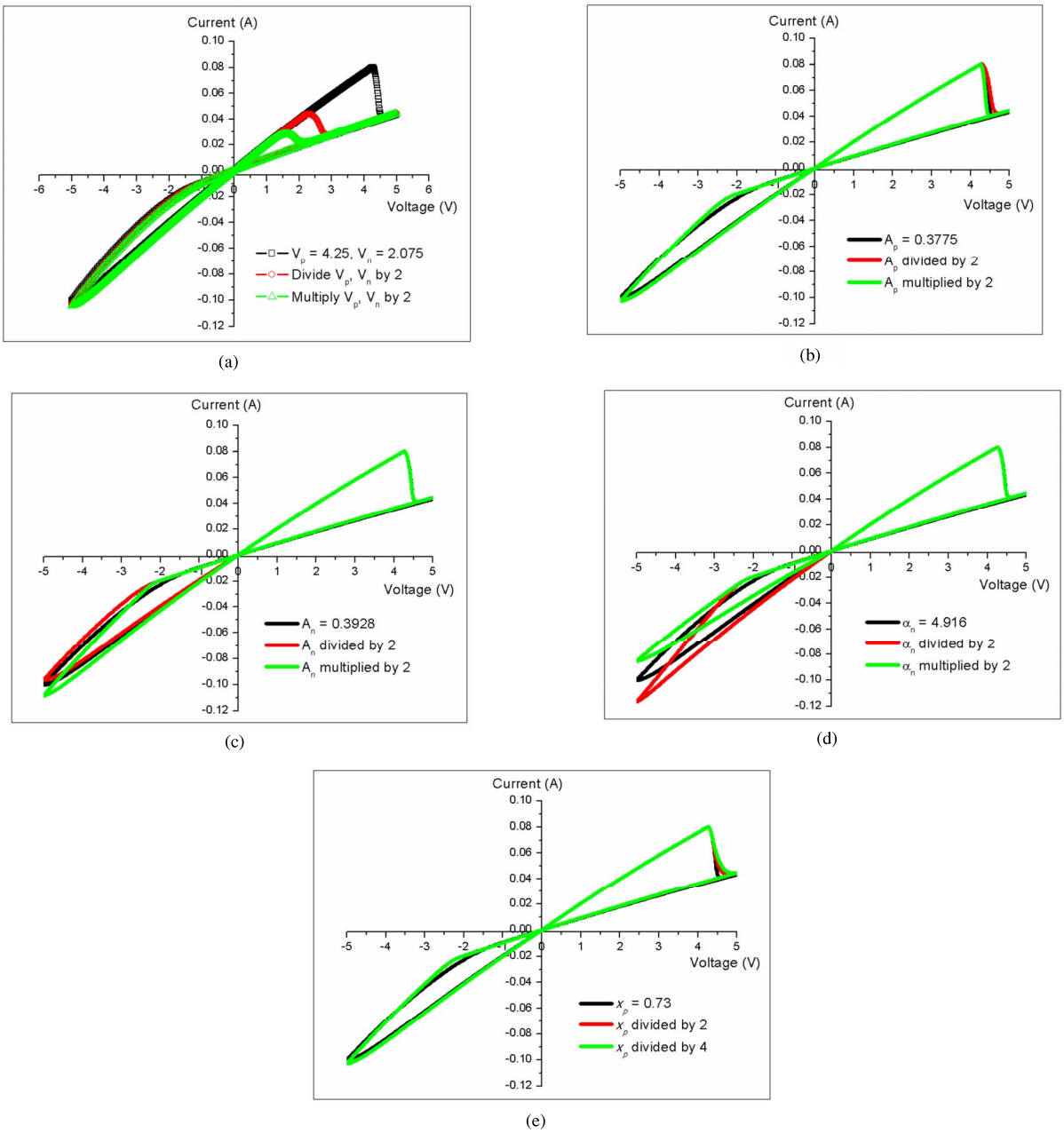

FIGURE 12. I-V characteristic of TiO_2 thin film annealed at 250°C for 20 min simulated using variations of I-V characteristic of TiO_2 thin film annealed at 250°C for 20 min simulated using variations of (a) V_p and V_n (b) A_p (c) A_n (d) α_n and (e) x_p.

Unlike α and β, the increasing and decreasing of γ and δ only cause the minimum positive current to change. This will subsequently leads to the modification of hysteresis loop area. The graphs in Figs. 11 a and b show that the shrinkage of hysteresis loop was obtained when γ and δ was multiplied by two. The loop however becomes larger when both

TABLE 4. R_{ON} and R_{OFF} With γ and δ Multiplied and Divided by Two.

		γ and δ divided by 2		γ and δ multiplied by 2	
	SIMULATION DATA FOR 250°C	γ (0.2238)	δ (0.0064)	γ (0.895)	δ (0.0256)
$R_{ON}(\Omega)$	52.97	52.77	52.77	52.77	52.77
$R_{OFF}(\Omega)$	113.29	144.77	144.77	75.03	75.03
R_{OFF}/R_{ON}	2.14	2.74	2.74	1.42	1.42

values decrease. As indicated in equation (5), γ and δ are related to the tunneling mechanism when memristor is in ON state.

By comparing the equation (5) with equation (12), the parameters γ and δ are thus given by $2nqv\exp(-\frac{\phi_B}{k_0T})$ and $\frac{aq}{k_0Td}$ respectively. If the barrier height is remain unchanged, the parameter γ will therefore influenced by the probability of electron transition without the barrier, v [43]. High value of v will result in the increase of the minimum positive current from 0.0358 A to 0.0548 A. This is due to the rise of the number of electron penetration through the barrier.

As a result the OFF state resistance is minimized and an ohmic like behavior will be achieved. Table 4 summarized the ON and OFF state resistances and R_{OFF}/R_{ON} ratio for γ and δ values multiplied and divided by two. From the data in Table 4 it is clearly seen that there is significant decrease of R_{OFF} value with the increase of γ.

In contrast to γ, δ value is influenced by the change of parameter a and the thickness of the device, d. Since, δ is inversely related to d, using thinner device will lead to the increases of δ and subsequently the memristance. As the parameter a is proportionally related to $\sqrt{\frac{1}{N_D}}$, the changes in the concentration of oxygen vacancies, N_D will lead to the modification of the hysteresis loop [43]. Therefore, the increase of oxygen vacancy concentration in memristive device resulted in the decrease of a and δ values. However, a larger area of hysteresis loop can still be achieved due to the increases of N_D.

From the above discussion, it can be concluded that the tunneling (γ and δ) and Schottky (α and β) current conductions are highly dependent on the parameters given in equation (12) and (19) respectively. These parameters can be categorized into two types: constant and physical parameters. The constants for example Boltzman constant, electron charge and others are the values which are independent to device structure. The physical parameters (e.g., top electrode area, thickness of the oxide layer, concentration of oxygen vacancies, etc) are the variables acquired from the properties of memristor. The initial predictive value of α, β, γ and δ can therefore be obtained by substituting the constant and physical parameters into the equation (12) and (19). The proposed model I-V characteristic will then compare to the experimental data and optimized for the best fitted plot. The root mean square errors will be consequently calculated.

B. THE STATE VARIABLE PARAMETER EFFECTS

The graphs in Figs. 12 a-e show the effects of state variable parameters variation on the I-V characteristic. The changes in positive threshold voltage become more pronounced with the changes in V_p and V_n. When observing the two plots in Figs. 12 b and e, the variations in A_p and x_p cause no changes in the I-V curve shape. Increasing and decreasing the values of A_n and α_n on the other hand cause the maximum negative current to vary. It is clearly seen that there were no significant modification of hysteresis loop was observed. This is because of the modeled state variable does not fully account for the physical charge transport mechanisms in memristor.

VI. CONCLUSION

The present correlation study was performed to identify the memristor SPICE models that are well fitted to the experimental data. The simulated models were hyperbolic-sine function based models. The models were correlated with I-V characteristics of sol-gel derived TiO_2 thin film annealed at 250°C for 20 min. From the correlation study, the models with the lowest root mean square errors were further simulated at different frequencies and using a DC input voltage for models validation. As Chang and Yakopcic models could produce a shrink of hysteresis loop area at higher frequencies and resulted in the lowest RMS errors when simulated using DC input voltage, they were then combined together and compared with TiO_2 thin films annealed at 350°C and 450°C to study the relationship between the model parameters and fabrication process conditions. Based on the fitting parameters, it was determined that the values of Schottky and tunneling parameters affected the conduction mechanism in the annealed TiO_2 thin film. The state variable parameters, on the other hand showed a strong relation to the device threshold voltage. The knowledge gained from the fabrication process condition and model parameter relationship enables us to predict the performance of memristive devices in various applications and subsequently allows a desired memristive behavior to be fabricated. Although the proposed combined model could accurately fit with our experimental data, how well the model account for the charge transport mechanism in TiO_2 memristive devices is questionable and hence require further investigation.

ACKNOWLEDGMENT

The authors would like to thank all members of NANO-Electronic Centre (NET), Universiti Teknologi MARA, Malaysia for their cooperation and support. Also thanks to Institute of Research Management and Innovation (IRMI), Universiti Teknologi MARA, Malaysia.

REFERENCES

[1] R. S. Williams, "How we found the missing memristor," *IEEE Spectr.*, vol. 45, no. 12, pp. 28–35, Dec. 2008.

[2] Q. Xia, "Nanoscale resistive switches: Devices, fabrication and integration," *Appl. Phys. A, Solids Surf.*, vol. 102, no. 4, pp. 955–965, Mar. 2011.

[3] R. Tetzlaff and T. Schmidt, "Memristors and memristive circuits: An overview," in *Proc. IEEE Int. Symp. Circuits Syst.*, Seoul, South Korea, 2012, pp. 1590–1595.

[4] H. Mahmoudi, V. Sverdlov, and S. Selberherr, "Novel memristive charge- and flux-based sensors," in *Proc. 8th Conf. Ph.D. Res. Microelectron. Electron.*, 2012, pp. 1–4.

[5] M. Potrebic and D. Tosic, "Application of memristors in microwave passive circuits," *Radioengineering*, vol. 24, no. 2, pp. 408–419, Jul. 2015.

[6] S. Hamdioui *et al.*, "Memristor based computation-in-memory architecture for data-intensive applications," in *Proc. Design Autom. Test Eur. Conf. Exhibit.*, Grenoble, France, 2015, pp. 1718–1725.

[7] Q. Li, A. Serb, T. Prodromakis, and H. Xu, "A memristor SPICE model accounting for synaptic activity dependence," *J. PLoS ONE*, vol. 10, no. 3, pp. 1–12, Mar. 2015.

[8] N. Z. Haron, N. Arshad, and F. Salehuddin, "Performance analysis of memristor models for RRAM cell array design using SILVACO EDA," *J. Technol.*, vol. 68, no. 3, pp. 1–6, 2014.

[9] S. M. M. Kasim, N. A. A. Shaari, R. A. Bakar, and S. H. Herman, "Switching behavior of titania-zinc oxide composites thin films," *Appl. Mech. Mater.*, vol. 749, pp. 308–312, Apr. 2015.

[10] N. S. Kamarozaman, Z. Aznilinda, S. H. Herman, R. A. Bakar, and M. Rusop, "Effect of annealing duration on the memristive behavior of Pt/TiO_2/ITO memristive device," in *Proc. 10th IEEE Int. Conf. Semicond. Electron. (ICSE)*, Sep. 2012, pp. 703–706.

[11] N. A. A. Shaari, S. M. M. Kasim, N. S. M. Sauki, and S. H. Herman, "The effect of the sol-gel spincoating deposition technique on the memristive behaviour of ZnO-based memristive device," in *Proc. 4th Int. Conf. Electron Device Syst. Appl.*, Kuala Lumpur, Malaysia, 2015, pp. 1–8.

[12] K. N. Pham, V. D. Hoang, C. V. Tran, and P. T. Phan, "TiO_2 thin film based transparent flexible resistive switching random access memory," *Adv. Nat. Sci Nanosci. Nanotechnol.*, vol. 7, no. 1, pp. 1–3, 2016.

[13] C. Chen, X. Yang, and F. Z. Wang, "An omnipotent memristor model with controllable window function," in *Proc. 17th UKSIM-AMSS Int. Conf. Model Simulat.*, 2015, pp. 600–605.

[14] M. M. Rehman *et al.*, "Resistive switching in all-printed, flexible and hybrid MoS_2-PVA nanocomposite based memristive device fabricated by reverse offset," *Sci. Rep.*, vol. 6, Nov. 2016, Art. no. 36195.

[15] V. Saminathan and K. Paramasivam, "Missing fourth element memristor modeling with new window function derived from sigmoid logistic equation," *Int. J. Adv. Eng. Technol.*, vol. 1, no. 1, pp. 384–386, 2016.

[16] A. Solak and S. Herdem, "A piece wise linear memristor model with switches," *Int. J. Model Opt.*, vol. 6, no. 2, pp. 124–127, 2016.

[17] K. Agashe, N. Sarwade, S. Joshi, and P. Soman, "Comprehensive study of current controlled memristor models," *Int. J. Sci. Eng. Res.*, vol. 7, no. 2, pp. 1376–1381, 2016.

[18] D. G. Ayana *et al.*, "Sol-gel derived oriented multilayer ZnO thin films with memristive response," *Thin Solid Film*, vol. 615, pp. 427–436, Sep. 2016.

[19] D. Panda, P. P. Sahu, and T. Y. Tseng, "A collective study on modeling and simulation of resistive random access memory," *Nanoscale Res. Lett.*, vol. 13, no. 8, pp. 1–48, 2018.

[20] F. Gul and H. Efeoglu, "Bipolar resistive switching and conduction mechanism of an Al/ZnO/Al-based memristor," *Superlattices Microstruct.*, vol. 101, pp. 172–179, Jan. 2017.

[21] M. H. Boratto, R. A. Ramos, Jr., M. Congiu, C. F. O. Graeff, and L. V. A. Scalvi, "Memristive behavior of the SnO_2/TiO_2 interface deposited by sol-gel," *Appl. Surface Sci.*, vol. 410, pp. 278–281, Jul. 2017.

[22] S. Benderli and T. A. Wey, "On SPICE macromodelling of TiO_2 memristors," *Electron. Lett.*, vol. 45, no. 7, pp. 377–379, Mar. 2009.

[23] S. Kvatinsky *et al.*, "Models of memristors for SPICE simulation," in *Proc. IEEE 27th Conf. Elect. Electron. Eng. Israel*, 2012, pp. 1–5.

[24] S. Kvantinsky, E. G. Friedman, A. Kolodny, and U. C. Weiser, "TEAM: Threshold adaptive memristor model," *IEEE Trans. Circuits Syst. I, Reg. Papers*, vol. 60, no. 1, pp. 211–221, Jan. 2013.

[25] D. B. Strukov, G. S. Snider, D. R. Stewart, and R. S. Williams, "The missing memristor found," *Nature*, vol. 453, no. 7191, pp. 80–83, May 2008.

[26] Y. N. Joglekar and S. J. Wolf, "The elusive memristor: Properties of basic electrical circuits," *Eur. J. Phys.*, vol. 30, no. 4, pp. 661–684, 2009.

[27] Z. Biolek, D. Biolek, and V. Biolková, "SPICE model of memristor with nonlinear dopant drift," *Radioengineering*, vol. 18, no. 2, pp. 210–214, 2009.

[28] T. Prodromakis, B. P. Peh, C. Papavassiliou, and C. Toumazou, "A versatile memristor model with nonlinear dopant kinetics," *IEEE Trans. Electron Devices*, vol. 58, no. 9, pp. 3099–3105, Sep. 2011.

[29] H. Abdalla and M. D. Pickett, "SPICE modeling of memristors," in *Proc. IEEE Int. Symp. Circuits Syst. (ISCAS)*, 2011, pp. 1832–1835.

[30] M. Laiho, E. Lehtonen, A. Russel, and P. Dudek, "Memristive synapses are becoming a reality," *Neuromorph. Eng.*, pp. 1–3, Nov. 2010.

[31] T. Chang *et al.*, "Synaptic behaviors and modeling of a metal oxide memristive device," *Appl. Phys. A, Solids Surf.*, vol. 102, no. 4, pp. 857–863, 2011.

[32] K. Eshraghian *et al.*, "Memristive device fundamentals and modeling: Applications to circuits and systems simulation," *Proc. IEEE*, vol. 100, no. 6, pp. 1991–2007, Jun. 2012.

[33] C. Yakopcic, M. T. Taha, G. Subramanyam, and R. E. Pino, "Memristor SPICE model and crossbar simulation based on devices with nanosecond switching time," in *Proc. Int. Conf. Neural Netw.*, 2013, pp. 464–470.

[34] R. E. Pino *et al.*, "Compact method for modeling and simulation of memristor devices: Ion conductor chalcogenide-based memristor devices," in *Proc. IEEE/ACM Int. Symp. Nanoscale Archit.*, 2010, pp. 1–4.

[35] A. Amirsoleimani *et al.*, "Accurate charge transport model for nanoionic memristive devices," *Microelectron. J.*, vol. 65, pp. 49–57, Jul. 2017.

[36] N. S. Kamarozaman *et al.*, "Effect of post-deposition annealing process on the resistive switching behavior of TiO_2 thin films by sol-gel method," *Adv. Mater. Res.*, vol. 925, pp. 125–129, Apr. 2014.

[37] O. Kavehei *et al.*, "The fourth element: Characteristics, modelling and electromagnetic theory of the memristor," *Proc. Roy. Soc. A Math. Phys. Eng. Sci.*, vol. 466, no. 2010, pp. 2175–2202, 2120.

[38] H. Li *et al.*, "Resistive switching characteristics of ZnO based ReRAMs with different annealing temperatures," *Solid-State Electron.*, vol. 75, pp. 28–32, Sep. 2012.

[39] C. M. S. Yakopcic, "Memristor device modeling and circuit design for read out integrated circuits, memory architectures, and nueromorphic systems," Ph.D. dissertation, School Eng., Univ. Dayton, Dayton, OH, USA, 2014. [Online]. Available: https://etd.ohiolink.edu

[40] E. Linn, A. Siemon, R. Waser, and S. Menzel, "Applicability of well-established memristive models for simulations of resistive switching devices," *IEEE Trans. Circuits Syst. I, Reg. Papers*, vol. 61, no. 8, pp. 2402–2410, Aug. 2014.

[41] T. Chang, "Tungsten oxide memristive devices for neuromorphic applications," Ph.D. dissertation, Dept. Elect. Eng., Univ. Michigan, Ann Arbor, MI, USA, 2012. [Online]. Available: https://deepblue.lib.umich.edu

[42] J. J. Yang *et al.*, "Memristive switching mechanism for metal/oxide/metal nanodevices," *Nat. Nanotech.*, vol. 3, pp. 429–433, Jun. 2008.

[43] W. Xiao-Ping, C. Min, and S. Yi, "Switching mechanism for TiO_2 memristor and quantitative analysis of exponential model parameters," *Chin. Phys. B*, vol. 8, no. 8, 2015, Art. no. 088401.

[44] L. O. Chua and S. M. Kang, "Memristive devices and systems," *Proc. IEEE*, vol. 64, no. 2, pp. 209–223, Feb. 1979.

[45] F. Zhang *et al.*, "The unification of filament and interfacial resistive switching mechanisms for titanium dioxide based memory devices," *J. Appl. Phys.*, vol. 109, no. 10, 2011, Art. no. 104504.
[46] J.-J. Huang, C.-W. Kuo, W.-C. Chang, and T.-H. Hou, "Transition of stable rectification to resistive-switching in Ti/TiO_2/Pt oxide diode," *Appl. Phys. Lett.*, vol. 96, no. 26, 2010, Art. no. 262901.
[47] K. Shubham and R. U. Khan, "Electrical characterization of TiO_2 insulator based Pd/TiO_2/Si MIS structure deposited by sol-gel process," *J. Nano Elect. Phys.*, vol. 5, no. 1, 2013, Art. no. 01021.
[48] E. W. Lim and R. Ismail, "Conduction mechanism of valence change resistive switching memory: A survey," *Electronics*, vol. 4, no. 3, pp. 586–613, 2015.
[49] Z. Jing and H. Da, "The influences of model parameters on the characteristics of memristors," *Chin. Phys. B*, vol. 21, no. 4, 2012, Art. no. 048401.
[50] Y. M. Reddy, M. K. Nagaraj, S. S. Naik, and V. R. Reddy, "Annealing effects on electrical properties and interfacial reactions of Ni/Cu Schottky rectifiers on n-type InP," *J. Mod. Phys.*, vol. 3, no. 7, pp. 538–545, 2012.
[51] A. Türüt, S. Tüzemen, M. Yildirim, B. Abay, and M. Saglam, "Barrier height enhancement by annealing Cr-Ni-Co alloy Schottky contacts on LEC GaAs," *Solid-State Electron.*, vol. 35, no. 10, pp. 1423–1426, 1992.
[52] D. A. Neamen, *Semiconductor Physics and Devices: Basic Principles*, 2nd ed. New York, NY, USA: McGraw-Hill, 1997, pp. 136–141.
[53] R. T. Tung, "The physics and chemistry of the Schottky barrier height," *Appl. Phys. Rev.*, vol. 1, no. 1, 2014, Art. no. 011304.
[54] H. Zheng *et al.*, "Barrier modification of metal-contact on silicon by sub-2 nm platinum nanoparticles and thin dielectrics," *Sci. Rep.*, vol. 6, Apr. 2016, Art. no. 25234.
[55] V. L. Devi, I. Jyothi, V. R. Reddy, and C.-J. Choi, "Schottky barrier parameters and interfacial reactions of rapidly annealed Au/Cu bilayer metal scheme on N-type InP," *Open Appl. Phys. J.*, vol. 5, pp. 1–9, Mar. 2012.
[56] M. L. Lee, J. K. Sheu, and S. W. Lin, "Schottky barrier heights of metal contacts to *n*-type gallium nitride with low-temperature-grown cap layer," *Appl. Phys. Lett.*, vol. 88, no. 3, 2006, Art. no. 032103.
[57] Ö. Güllu, "Barrier modification by methyl violet organic dye molecules of Ag/P-InP structures," *Eur. J. Interdisciplinary Stud.*, vol. 5, pp. 7–17, May/Aug. 2016.
[58] R.-H. Chang *et al.*, "Surface modification on the sputtering-deposited ZnO layer for ZnO-based Schottky diode," *J. Nanomater.*, vol. 2013, Nov. 2013, Art. no. 560542.
[59] V. Janardhanam, Y.-H. Kil, K.-H. Shim, V. R. Reddy, and C.-J. Choi, "Effect of rapid thermal annealing on the electrical and structural properties of the Se Schottky contacts to n-type Si," *Mater. Trans.*, vol. 54, no. 7, pp. 1067–1072, 2013.
[60] C.-Y. Wang, H.-P. Shiao, P.-W. Shieh, and H.-H. Chang, "Thermal annealing effects on electrical and structural properties for Ni-Au/n-GaN Schottky contacts," *Appl. Mech. Mater.*, vols. 284–287, pp. 241–244, Jan. 2013.
[61] H. Lin-Chao *et al.*, "Annealing temperature influence on the degree of inhomogeneity of the Schottky barrier in Ti/4H-SiC contacts," *Chin. Phys. B*, vol. 23, no. 12, 2014, Art. no. 127302.
[62] A. N. Corpus-Mendoza, M. M. De Souza, and F. Hamelmann, "Transport mechanisms and effective Schottky barrier height of ZnO/a-Si:H and ZnO/μc-Si:H heterojunction solar cells," *J. Appl. Phys.*, vol. 114, no. 18, 2013, Art. no. 184505.

RAUDAH ABU BAKAR received the B.Eng. degree from the University of Surrey, U.K., in 2002 and the M.Sc. degree from Universiti Teknologi MARA, Malaysia, in 2008, where she is currently pursuing the Ph.D. degree.

NUR SYAHIRAH KAMAROZAMAN received the B.Eng. (Hons.) and M.Sc. degrees in science electrical engineering from Universiti Teknologi MARA, Malaysia, in 2011 and 2015, respectively. She is currently a Lecturer with the Faculty of Electrical Engineering, Universiti Teknologi MARA, Terengganu Campus, Malaysia.

WAN FAZLIDA HANIM ABDULLAH received the B.Eng (Hons.) degree in electronics engineering from the University of Southampton in 1993, the M.Sc. degree in electronic engineering from Universiti Putra Malaysia in 2002, and the Ph.D. degree in microengineering and nanoelectronics from Universiti Kebangsaan Malaysia in 2010. She is an Assistant Professor with the Faculty of Electrical Engineering, Universiti Teknologi MARA, Malaysia. Her research interests include microelectronic devices, solid-state sensors, and nanoelectronics and sensor interfacing circuits. Her recent projects are extended-gate field-effect transistor sensor readout circuitry, multisensory environment with data analytics, and ROICs for amperometric DNA biosensors.

SUKREEN HANA HERMAN received the B.Eng. degree in electrical, electronics, and information engineering and the M.Eng. degree in electronics and computer science from Kanazawa University, Japan, in 1999 and 2004, respectively, and the Ph.D. degree in materials science from the Japan Andvanced Institute of Science and Technology, in 2009. She received the Malaysian Public Service Department Scholarship for her degree, the Panasonic Scholarship for her master's degree, and the Japan Monbukagakusho Scholarship for her Ph.D. degree.

She was with Sharp-Roxy. She joined Universiti Teknologi MARA in 2004, where she is currently the Senior Lecturer with the Center for Electronic Engineering Studies, Faculty of Electrical Engineering and heads the Integrated Sensor Research Group. Her research interests include fabrication and characterization of semiconductor materials, sensing membranes, and nanostructured materials. Although her work explores various methods of fabrication and growth, her early work focused on sputtering deposition where she designed and developed an RF sputtering machine for her master's research.

Dr. Herman has authored over 170 articles and conference proceedings. She was a recipient of various major awards in invention and innovation exhibition and competitions.